Multidisciplinary Review Journal

Journal of Critical Reviews

ISSN- 2394-5125 Vol 7, Issue 2, 2020

Review Article

PERCEPTUAL MASKING BASED MEDICAL IMAGE WATERMARKING USING DTCWT AND HVS

[1]Kavitha V, [2]Palanisamy C, [3]Sureshkumar T

[1]Nandha College of technology,Erode-638052, kavithamebit@gmail.com,
[2]Bannari amman college of technology,Sathyamangalam-638401, cpalanisamy@gmail.com
[3]Er.Perumal Manimekalai College of engineering,Hosur-635117, sureshkumar@ksrct.ac.in

Received:30.11.2019 *Revised: 16.12.2019* *Accepted: 19.01.2020*

Abstract
In this paper, a DTCWT based perceptual watermarking scheme for medical images is proposed. The imperceptibility characteristic is ensured using a new proposed perceptual masking model. Both the host image and the cover image are decomposed using 2level DTCWT. The quantization for the selected subband coefficients for embedding is measured using HVS mathematical model which produces the watermark weighing function. The method is experimented for its performance against common attacks and the results have proven that the model was robust to withstand most of the attacks.

Keywords: medical image compression, DTCWT, HVS

DOI: http://dx.doi.org/10.31838/jcr.07.02.104

INTRODUCTION

In the modern medical world, the health care institutions are required to provide state of the art medical care facilities to the patient, which sometimes requires transmitting of medical data in the electronic media. Once the medical data ventures into the cyberspace, it is prone to security issues as any other data in transit. A better way to address these issues is through watermarking, which addresses the issues using security principles that ensure the reliability, authenticity and security of the data transmitted. Further, adopting a watermarking technique to protect the medical data transmitted must adhere to the standards and laws established by the medical council of any province through a legislature. Moreover, the watermarking techniques must secure the image from any form of attacks.The ability to embed the watermark image in an irregular fashion all throughout the host image after inversely transformed had made the transform domain-based methods more resilient against common geometric, noise and compression attacks when compared with the spatial domain-based algorithms. The main drawback of the transform domain-based approaches is the limit in the capacity of the watermark images to be embedded is less as against the spatial domain watermarking schemes.

One of the most successful transform domain techniques is Discrete Wavelet Transform [Mousavi SM et al. 2014]. The popularity of the method is attributed to its time-frequency features based on Human Visual System. [Adhipathi Reddy et al. 2005] As for the application in this proposed work, the medical image representation requires high image quality even after the watermark embedding, while maintaining the capacity of the watermark. [Giakoumaki et al. 2006]. However successful the DWT may be, yet it suffers from two significant setbacks, one is that it lacks shift invariance, which results in excessive scaling of DWT coefficients even for a little shift in input data signal. Moreover, the second setback is that it does not support the directional selectivity for diagonal features. [Kingsbury NG 2001]

These drawbacks are better encountered by a new type of transform named Dual-Tree Complex Wavelet Transform (DTCWT) which was proposed by Kingsbury NG 1998 The proposed technique was a combination of advantageous features from both DWT and CWT (Complex Wavelet Transform). These combinations have made the proposed transform technique more reliable as it delivers i) better selection of direction, ii) utmost shift invariance, iii) ideal image reconstruction, iv) reduced complexity and v) reduced repetitions [Kingsbury NG 2001]. Owing to these attributes the embedding methods built using Dual-Tree Complex Wavelet Transform had outshined other transform based watermarking systems.

In this paper, a DTCWT based perceptual watermarking scheme for medical images is proposed. The imperceptibility characteristic is ensured using a new proposed perceptual masking model. The model is based on the work of Zebbiche K et al, 2014, which is enhanced to work in DTCWT domain. The proposed model adapts to the HVS features such as i) brightness sensitivity, ii) texture sensitivity, iii) Contrast sensitivity, iv) Frequency sensitivity and direction sensitivity. This adaptation helps to ensure the quantification in the level of unnoticeable distortions in the watermarked image.

PRELIMINARIES

Dual Tree Complex Wavelet Transform (DTCWT)

The idea behind DTCWT is that it employs dual filter trees to generate dual bands of coefficients, these dual coefficients are grouped to generate complex coefficients. Practically speaking the DTCWT employs two DWTS each employing a different set of filters for generating the coefficients. The first DWT with its filter set generates the real part of the transform and the imaginary part of the transform is generated using the second part of DWT and its filters, due to this is the reason the DTCWT generates redundant coefficients, which are scaled using a factor of 2n for n-dimensional transforms. During the inverse operation of the DTCWT, the real and the imaginary part are inversed using the two inverse of real DWTs that in turn generates two real signals. The final resultant signal is the average of the two real signals previously generated [Selesnick et al.2005].

For an input image signal img(s) the one level DTCWT as shown in figure 1, transforms the image signal into a complex mother

wavelet ∂(s) and a scaling function ϑ (s), the following equation represents the 1D-DTCWT transformation for any given signal,

$$img(s) = \sum_{n\in X} M_{k_o,n}\vartheta_{k_o,n}(s) + \sum_{k\geq k_0}\sum_{n\in X} P_{k,n}\partial_{k,n}(s) \quad (1)$$

In the above equation 4.1, the scaling and wavelet coefficients are represented using the notations $M_{k_o,n}$ and $P_{k,n}$ respectively. Both the coefficients have real and imaginary part represent as $\vartheta_{k_o,n}$ and $\partial_{k,n}$.

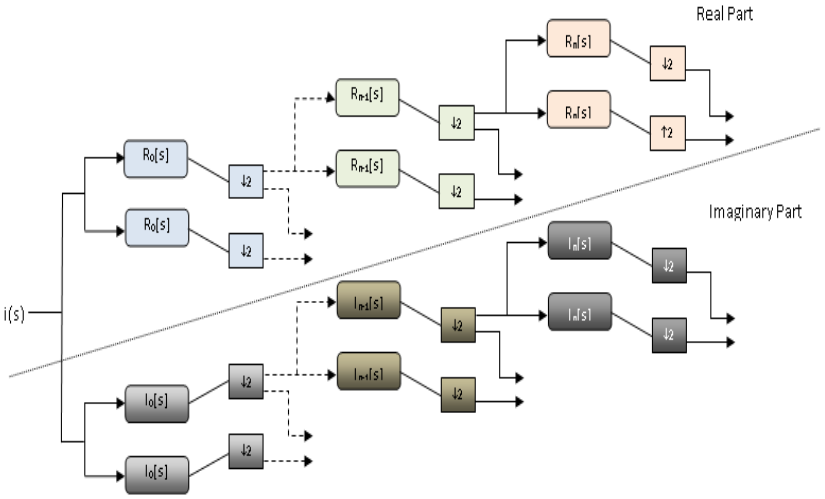

Fig. 1:1-D dual-tree complex wavelet transform

The DTCWT produces two low-frequency complex subbands and six complex high-frequency subbands for 2D input signals for every level of transformation. The sixhigh-frequency subbands are oriented at ±15◦, ±45◦ and ±75◦ angles as directional filters [Coria et al. 2008]. The decomposed low-frequency subbands can be mathematically represented as:

$$a(\alpha, Lw_f, x, y) = Tr\left(a(\alpha, Lw_f, x, y)\right) + hFa\left(a(\alpha, Lw_f, x, y)\right) \quad (2)$$

in which Lwf∈{Lw_1, Lw_2} and the high-frequency subbands can be expressed as:

$$a(\Delta, \tau, x, y) = Tr(a(\Delta, \tau, x, y)) + hFa(a(\Delta, \tau, x, y)) \quad (3)$$

In both the high and low-frequency subband equations the real and imaginary parts are correspondingly denoted using Tr and Fa notations. The DTCWT generates low-frequency subbands at first and second level of transformation which is represented as Lw_1 and Lw_2. The DTCWT transformation level is represented using Δ, and the direction of the subband is represented using τ. The input image size used for the decomposition is represented using j, k and the values of the location are represented using x and y.

Human Visual System

For the human brain to perceive the outside world is done through the human visual system. In the electromagnetic spectrum, the visible light spectrum is just a marginal spectrum among the other spectrums like x-rays, gamma rays, ultraviolet rays, infrared rays etc. Our visual system is built to respond and perceive only to the visual light portion of the electromagnetic spectrum [Huiyan et al. 2008]. The visual light spectrum is denoted using the wavelength (γ) that lies within the frequency band ranging between 350nm to 780nm. The light reception reflected through an object can be expressed as the product of reflectivity of the object and incident energy distribution for the light to get transmitted through the object, which is given by

$$L(\gamma)=R(\gamma)\,E(\gamma), \quad (4)$$

where R(γ) is the reflectivity of the object, which takes the value between 0 and 1.

Spectral Sensitivity

The Spectral Sensitivity for any light source can be termed as the wavelength function γ related to its light intensity. In nature, the human visual system has been gifted with a low pass filter in the form of the pupil of the eye that acts as an aperture. Usually, the low pass filter of the eye can detect the bright light band of about 60 cycles per degree. It is quite natural that the eye is not such sensitive to the luminance and more sensitive to the contrast, this is stated through Weber's law for luminance, which states that, for a visually different luminance of an object g_o with respect to its surrounding luminance g_s is represented as a ratio using the function:

$$\frac{|g_s - g_0|}{g_0} = 0.02, \quad (5)$$

here the value 0.02 is the constant for the ratio defined.

Contrast Sensitivity Function

Mannos and Sakrison 1974. defines the contrast sensitivity in terms of the reciprocal function of spatial frequency S in terms of visible contrast, with the maximum and minimum luminance corresponding to that spatial frequency is represented as I_{max} and $I_{min.}$, then the contrast T and the Contrast sensitivity function (CSF) TS for the spatial frequency f_s is expressed as

$$T = \frac{I_{max} - I_{min}}{I_{max} + I_{min}} \quad (6)$$

$$SF(S) = M_l.\left(1 + t_f.S\right).e^{(b.S)^{\beta}}, \quad (7)$$

Where M_l represents the mean luminance, t_f represents the temporal frequency and b, β represents the orientation.

Spatial Masking

The reduced perception of an image element resulted due to the incidence of another image signal in the same space is referred as the masking effect [Watson et al. 1997][Kein et al. 1997]. The masking effect explains the phenomenon that for a signal A to be perceived by the HVS is based on the strength of another signal B in the same vicinity, if the B's signal is strong then HVS perceives the signal B or else the signal A.This attributes to the facts generalized by works [DeYoe et al. 1988] that the vision is a parallel multi-channel, which means that the visual system could process different input elements through different neural systems parallel in the visual cortex. The next set of processing is done at independent channels of the cortical cells that analyze and forward the selection to the spatial memory of the HVS.

Human Visual System (HVS) in Image Watermarking

Profound studies on the HVS and the extent of scope it can be integrated into the watermarking field are reflected through the following characteristics:

a) The human visual system is found to exhibit band pass features, as per the studies conducted under Psycho Visual testing
b) The HVS has a different level of sensitivity that varies on the basis of variations in both resolution levels and directions.
c) Brightness and luminance also influence the sensitivity of HVS.
d) Being anisotropic the HVS shows a different level of sensitivity for different spatial and diagonal directions with the orientation of +45°.
e) The asymmetric errors are less susceptible to HVS detection than symmetric errors.
f) The noise distributions at high and local texture areas are less perceptive to the Human Visual Systems.
g) HVS is more perceptive towards the edges of an image, and it maintains the integrity of an image.
h) For entropy-based decomposition models like DTCWT, the subband coefficients are used to measure the roughness.

Properties of Human Visual System used in Present Work

Building an effective watermarking scheme using HVS, all the factors related to HVS must be considered for the designing, which is quite complicated. For the proposed work the following properties are taken into consideration with perception to the medical images.

Brightness Sensitivity

In medical images, the images like MRI and X-rays that cascades darker background and lighter objects are more sensitive towards brightness. The lighter and darker stature of the region in the image can be represented using pixel values, a pixel value of zero represents the darker intensity, and the pixel value of 255 corresponds to the brighter intensity. The mid-value between 0 to 255 corresponds to different mixtures of grey, this can be represented using the following equation.

$$\mathcal{E}(k,l,n) = \mathcal{L}_n^m(k,l) \quad (8)$$

Frequency Sensitivity

Incorporating the HVS into the embedding model requires multi-resolution analysis of the human vision. The analysis provides the understanding of Human vision's weakness and the way it can be capitalized in embedding the watermark signals into the decomposed coefficients of host image using DTCWT. Based on this understanding, a level parameter can be defined to reflect the level of decomposition that yields high frequency coefficients in which the embedding can be performed.

Direction Sensitivity

The studies on HVS shows that the visionary system is less sensitive in the diagonal orientation as against the other two orientations. The proposed model takes the advantage and uses these characteristics in terms of directional sensitivity to generate vertical, horizontal and diagonal attributes of the image into consideration for better watermarking. The watermark's strength varies in accordance with the direction of the decomposition. The direction parameter τ can have values 1,2 and 3 which represents diagonal, vertical and horizontal directions respectively.

PROPOSED METHODOLOGY

Watermark Embedding Process

In this proposed work's watermark embedding process as shown in figure 2, The steps for embedding are as follows.

1. In the first step, the image to be watermarked is decomposed using two-level DTCWT. The sub-band coefficients from the second level containing the higher frequency of the image are selected for embedding.
2. Simultaneously, two-level DTCWT is performed on the watermark image $Img_w$to obtain a low-frequency sub-band and six high-frequency subbands.
3. Subband coefficients from the higher frequency are selected based on the global parameter 'ρ' together with HVS parameters such as frequency sensitivity, direction sensitivity and brightness sensitivity (luminance).
4. The six-high frequency subband coefficients of the watermark image are then embedded into the six-high frequency subband coefficients of the host image selected based on the HVS characteristics.
5. Inverse DTCWT is applied over the coefficients to generate the watermarked image.

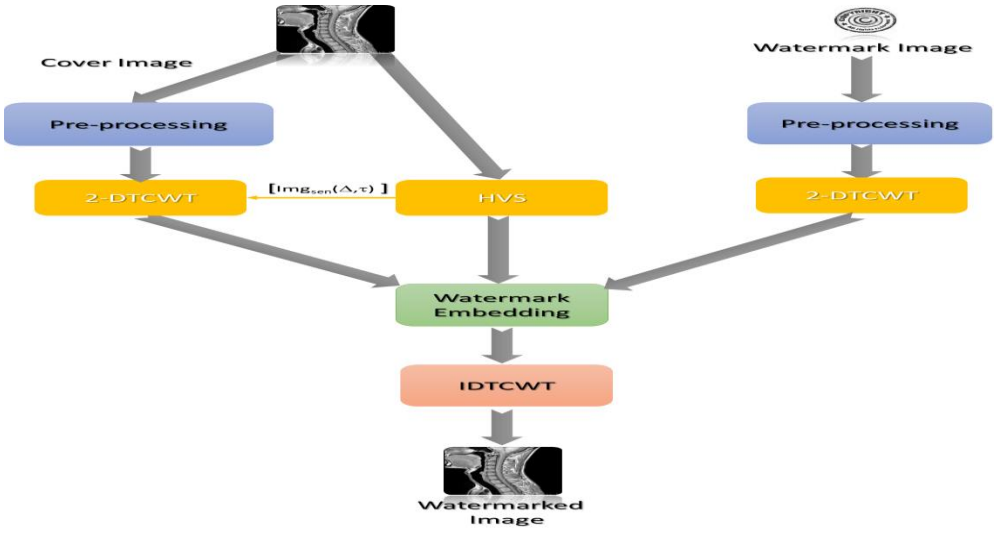

Fig 2 Embedding Process

WATERMARK EXTRACTION PROCESS

For the extraction process as shown in figure 3, the proposed scheme requires both the host image and the watermarked image. The watermarked image is subjected to two-level DTCWT to generate the required high-frequency subband coefficients. The watermark image is then extracted by applying appropriate correlation function and inverse 2DDWT function.

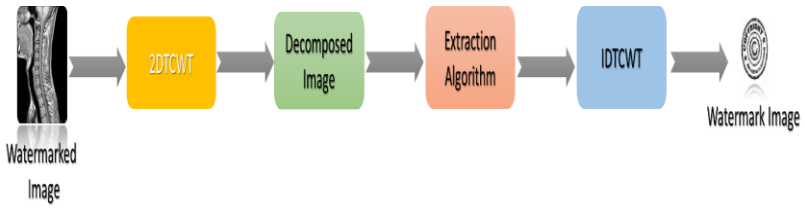

Fig 3 Extraction Process

1) Apply 2D-DTCWT to the watermarked image to decompose it to two levels of one low-frequency subband and six high-frequency subbands.
2) The sixhigh-frequency subbands in which the watermark is embedded is chosen and subjected to the following function

$$\mathrm{Img_w}^{*}(m,n) = \frac{W^{*}(m,n) - \mathrm{Img}(m,n)}{\rho\Delta(m,n) * \mathrm{Img_{sen}}(\Delta,\tau)} \quad (9)$$

3) Apply inverse 2D-DWT on the $\mathrm{Img_w}^{*}(m,n)$ to generate the actual watermark image $\mathrm{Img_w}(m,n)$.

EXPERIMENTAL RESULTS AND DISCUSSION

The watermarking model presented in this chapter is experimented and evaluated through Matlab software using the same set of medical images such as X-ray, US, MRI, and CT. The images are sourced from Rider Neuro MRI database for experimental purpose. The robustness, imperceptibility and security are measured through three experiments, which are discussed in the following section.

Experiment #1: Against Geometric Attacks

In this experiment, the proposed model's ability has been tested against various geometric attacks. The geometric attacks are also referred to as de-synchronization attacks that try to make the watermark detection process subtler by including operations like rotation, translation, scaling and cropping etc. In the proposed work the watermarked images are examined by subjecting to the attacks including i) cropping, ii) Rotation (90° clockwise), and iii) sharpening.

Cropping

The cropping attack is the most common and the easiest of geometric attack used on the watermarked image. In this work the watermarked images are cropped 15% at the top left corner, top right corner, bottom left corner and bottom right corners. The PSNR and SSIM comparison is shown in table 1.

Table 1 PSNR and SSIM values for the watermarked images against cropping attacks

Cropping Attack (15%)	img#001		img#002		img#003	
	PSNR	SSIM	PSNR	SSIM	PSNR	SSIM
No attack	46.08	0.9891	41.98	0.9735	39.81	0.9463
Top left corner	37.09	0.9317	33.02	0.9426	30.28	0.9221
Top right corner	37.01	0.9309	33.75	0.943	31.01	0.9268
Bottom right corner	36.77	0.9271	32.4	0.9314	32.88	0.9351
Bottom left corner	36.82	0.9287	32.57	0.9706	32.68	0.9316

Rotation

The rotation geometric attack involves rotating the watermarked image in different angles. In this work, for the experimentation purpose, all the three images are rotated in three different angles 90°, 180° and 270°. The PSNR and SSIM values are shown in table 2.

Table 2 PSNR and SSIM values for the watermarked images against rotation attacks

Rotation Attack	img#001		img#002		img#003	
	PSNR	SSIM	PSNR	SSIM	PSNR	SSIM
No attack	46.08	0.9891	41.98	0.9735	39.81	0.9463
90° right	38.01	0.9659	34.75	0.953	32.01	0.9368
180° right	37.91	0.9609	34.93	0.9571	32.21	0.9388
270° right	37.97	0.9671	34.46	0.9544	32.38	0.9391

Sharpening Attacks

The sharpening is fundamentally the execution of high pass filter to the watermarked image. In this work, the watermarked image is sharpened using 3 x 3 filter kernel. The PSNR and SSIM values are shown in table 3.

Table 3 PSNR and SSIM values for the watermarked images against sharpening attacks

Sharpening Attack	img#001		img#002		img#003	
	PSNR	SSIM	PSNR	SSIM	PSNR	SSIM
No attack	46.08	0.9891	41.98	0.9735	39.81	0.9463
Strength = 50	33.07	0.9671	31.4	0.9514	28.88	0.9351
Strength = 60	31.91	0.9601	30.53	0.9471	28.02	0.9313
Strength = 70	29.97	0.9571	29.46	0.9444	27.45	0.9291
Strength = 80	29.02	0.9501	28.96	0.9412	26.93	0.9276

Experiment #2:Against Compression attacks

In this experiment, all the watermarked images are evaluated against the JPEG compression attacks. The watermarked images are subjected to JPEG attacks under various quality factors. The PSNR and SSIM values are shown in table 4.

Table 4 PSNR and SSIM values for the watermarked images against compression attacks

Compression Attack	img#001		img#002		img#003	
	PSNR	SSIM	PSNR	SSIM	PSNR	SSIM
No attack	46.08	0.9891	41.98	0.9735	39.81	0.9463
Q = 90	36.82	0.9787	33.57	0.9706	30.68	0.9516
Q = 80	35.08	0.9719	33.06	0.9701	29.12	0.9507
Q = 70	33.63	0.9648	32.68	0.9619	29.26	0.9492
Q = 60	32.45	0.9457	30.94	0.9517	27.16	0.9317
Q = 50	30.07	0.9273	30.43	0.9319	24.79	0.9076

The approach is significantly robust against compression for quality factor Q > 50 and tends to lose the image integrity when Q < 40.

Experiment #3: Against Noise attacks

For the third and final experiment, the watermarked images are subjected to three types of noise attacks such as i) salt and pepper, ii) Speckle noise and iii) Gaussian noise. The following table shows the effects of various noise attacks over the watermarked images

Salt and Pepper noise

For the experimentation, the noise density was varied from 0.1 to 0.9, in increments of 0.2 which results in 5 different modalities for each watermarked image. The PSNR and SSIM values are shown in the table 5.

Table 5 PSNR and SSIM values for the watermarked images against salt & pepper noise

Salt and pepper Noise Attack	img#001		img#002		img#003	
	PSNR	SSIM	PSNR	SSIM	PSNR	SSIM
No attack	46.08	0.9891	41.98	0.9735	39.81	0.9463
density = 0.1 db	27.39	0.9714	27.87	0.9657	23.7	0.9486
density = 0.3 db	27.05	0.9703	27.16	0.9701	22.14	0.9416
density = 0.5 db	25.92	0.9694	26.12	0.9619	21.86	0.9377
density = 0.7 db	24.84	0.9687	25.74	0.9517	21.04	0.9324
density = 0.9 db	23.79	0.9643	24.82	0.9319	20.57	0.9276

Speckle Noise

The speckle noise is added to the image in increments of .15 from .15 to 0.90, which results in six attacked watermark images for each modality. The PSNR and SSIM values are shown in table 6.

Table 6 PSNR and SSIM values for the watermarked images against speckle noise

Speckle Noise Attack	img#001		img#002		img#003	
	PSNR	SSIM	PSNR	SSIM	PSNR	SSIM
No attack	46.08	0.9891	41.98	0.9735	39.81	0.9463
variance = 0.15	26.7	0.9707	27.12	0.9552	22.58	0.9363
variance = 0.30	26.46	0.9700	27.03	0. 9546	22.36	0.9351
variance = 0.45	25.95	0.9696	26.92	0.9527	22.21	0.9338
variance = 0.60	25.63	0.9694	26.72	0.9518	22.12	0.9325
variance = 0.75	25.14	0.9689	26.34	0.9505	22.04	0.9314
variance = 0.90	24.89	0.9681	26.02	0.9497	21.89	0.9299

Gaussian Noise

For the experiment, the mean is set at 1 and the variance was incremented by 0.002 from 0.001 to 0.009, which results in five noise images for each modality. The PSNR and SSIM values are shown in the table 7.

Table 7 PSNR and SSIM values for the watermarked images against Gaussian noise

Gaussian Noise Attack	img#001		img#002		img#003	
	PSNR	SSIM	PSNR	SSIM	PSNR	SSIM
No attack	46.14	0.989	42.01	0.9771	40.11	0.9479
variance = 0. 0.001	23.14	0.9427	23.11	0.9317	20.57	0.9128
variance = 0. 0.003	22.96	0.9419	22.99	0.9306	20.25	0.9114
variance = 0. 0.005	22.45	0.9396	22.52	0.9297	20.03	0.9100
variance = 0. 0.007	22.11	0.9379	22.18	0.9288	19.87	0.9092
variance = 0. 0.009	21.94	0.9359	21.97	0.9275	19.46	0.9081

Table 8 Comparison of PSNR and SSIM for three images against different types of attack.

Attack			img#001		img#002		img#003	
			PSNR	SSIM	PSNR	SSIM	PSNR	SSIM
No attack			46.08	0.9891	41.98	0.9735	39.81	0.9463
Geometric Attacks	**Cropping**		37.09	0.9317	33.02	0.9426	30.28	0.9221
	Rotation		38.01	0.9659	34.75	0.953	32.01	0.9368
	Sharpening		33.07	0.9671	31.4	0.9514	28.88	0.9351
JPEG Compression	**Q =**	**90**	36.82	0.9787	33.57	0.9706	30.68	0.9516
		80	35.08	0.9719	33.06	0.9701	29.12	0.9507
		70	33.63	0.9648	32.68	0.9619	29.26	0.9492
		60	32.45	0.9457	30.94	0.9517	27.16	0.9317
		50	30.07	0.9273	30.43	0.9319	24.79	0.9076
Noise	**Salt**		27.39	0.9714	27.87	0.9657	23.7	0.9486

Attacks	&Pepper						
	Speckle	26.7	0.9707	27.12	0.9552	22.58	0.9363
	Gaussian	22.67	0.9426	22.54	0.9315	20.09	0.9128

Table 8 gives a sum up of the overall performance of the proposed DTCWT-HVS model. As anticipated the model delivered better imperceptibility for all the images against the common attacks. The model displayed a better tradeoff between the robustness and imperceptibility. The average PSNR for the image img#001 was around 33.25, for image img#002 was around 31.6, and for the image img#003 it was around 28.19. the SSIM average stood around 0.96, 0.95 and 0.93 for the images img#001, img#002 and img#003 respectively. The PSNR and SSIM values shown above reflects that the model is quite satisfactory in terms of fulfilling the medical image watermarking requirements.

CONCLUSION

In this proposed work DTCWT and HVS based nonblind watermarking scheme is proposed. During the watermark embedding process, both the host image and the cover image are decomposed using 2level DTCWT. The higher frequency subbands are selected using HVS parameters, and the selected coefficients are used for the embedding. The higher frequency subband coefficients of the watermark are embedded into the selected coefficients of host image using a masking function.The experimental results have shown that the proposed scheme is more rigid and robust against compression, geometric and noise attacks as it employs HVS based perceptual masking for watermark embedding. The method is also more imperceptible to common attacks.

REFERENCES:

1. A. Giakoumaki, S. Pavlopoulos and D. Koutsouris, "Multiple Image Watermarking Applied to Health Information Management," in IEEE Transactions on Information Technology in Biomedicine, vol. 10, no. 4, pp. 722-732, Oct. 2006
2. Adhipathi Reddy and Biswanath N. Chatterji. 2005. A new wavelet based logo-watermarking scheme. Pattern Recognition Letters 26, 7 (2005), 1019–1027. DOI:http://dx.doi.org/10.1016/j.patrec.2004.09.047
3. Coria LE, Pickering MR, Nasiopoulos P, Ward RK (2008) A video watermarking scheme based on the dual-tree complex wavelet transform. IEEE Trans Inf Forensics Secur 3(3):466–474.
4. De Yoe, A. E., and Van Essen, C. D., "Concurrent processing streams in monkey visual cortex," Trends in Neurosciences, 11(5), 219-226 (1988).
5. Huiyan Qi, Dong Zheng, Jiying Zhao, " Human Visual System based Adaptive Digital Image watermarking", Elsevier Signal Processing, Vol. 88, Issue 1, 2008, pp. 174-188
6. Kein, A. S., Carney, T., Barghout-stein, L., and Tyler, W. C., "Seven models of masking," in Proc. SPIE, 3016, San Jose, CA, 13-24 (1997).
7. Kingsbury NG (1998) The dual-tree complex wavelet transform: a new technique for shift invariance and directional filters. In: IEEE digital signal processing workshop, Bryce Canyon
8. Kingsbury NG (2001) Complex wavelets for shift invariant analysis and filtering of signals. Journal of Applied and Computational Harmonic Analysis 10(3):234–253
9. L. Mannos, D. J. Sakrison, ``The Effects of a Visual Fidelity Criterion on the Encoding of Images'', IEEE Transactions on Information Theory, pp. 525-535, Vol. 20, No 4, (1974)
10. Mousavi SM, Naghsh A, Abu-Bakar SA. Watermarking techniques used in medical images: a survey. J Digit Imaging, 27(6), (2014), 714-29
11. Selesnick IW, Baraniuk RG, Kingsbury NG (2005) The dual tree complex wavelet transform: a coherent framework for multiscale signal and image processing. IEEE Signal Proc Mag 22(6):123–151
12. Watson Andrew B, Yang Gloria Y, Solomon Joshua A and Villasenor John 1997 Visibility of wavelet quantization noise. IEEE Trans. Image Process. 6(8): 1164–1175
13. Zebbiche K, Khelifi F (2014) Efficient wavelet-based perceptual watermark masking for robust fingerprint image watermarking. IET Image Process 8(1):23–32
14. Asha Jose, Elango Kannan, Palur Ramakrishnan Anand Vijaya Kumar, SubbaRao Venkata Madhunapantula. "Therapeutic Potential of Phytochemicals Isolated from Simarouba glauca for Inhibiting Cancers: A Review." Systematic Reviews in Pharmacy 10.1 (2019), 73-80. Print. doi:10.5530/srp.2019.1.12